

EVAPORATION-DRIVEN CHARGE REDISTRIBUTION AND CURRENT GENERATION FOR ENERGY HARVESTING APPLICATIONS

Ruba T. Borno and Joseph Steinmeyer

Department of Electrical Engineering and Computer Science
The University of Michigan
Ann Arbor, MI, 48109

Michel M. Maharbiz

Department of Electrical Engineering and Computer Science
University of California Berkeley
Berkeley, CA, 94720

ABSTRACT

The development of low power wireless sensor networks has generated interest in previously unsuitable energy harvesting methods as viable sources of power. We present a microfabricated synthetic leaf that can generate output voltages of 2 – 5 μV for each motion of a gas-liquid interface due to the mechanical energy of evaporation-driven flow. The presented results provide a proof of concept for the use of evaporation-driven flow as a scalable mechanism of electrical energy conversion and energy harvesting applications.

I. INTRODUCTION

Many scenarios and environments exist where evaporation of water, and the corresponding formation of humidity gradients, allow for energy to be scavenged. Examples include the surface of the skin due to perspiration, near the surface of bodies of water, and the soil-air interface which is utilized to do work via transpiration by the vast majority of plants on earth. The presented energy conversion system makes use of capacitor plates embedded in a synthetic leaf where electric current generated by the rapid change of a capacitor's dielectric constant due to interface motion is harvested by an on-chip circuit (Figure 1a-e).

We previously documented the change in capacitance as a result of the changing dielectric (Borno 2007). This work demonstrates the first measurement of electric currents, voltage outputs using a charge pump circuit, and further presents the characterization of fluidic parameters of the device. The presented results provide a proof of concept for the use of evaporation-driven flow as a mechanism of electrical energy conversion and energy harvesting applications.

2. ELECTROSTATIC TRANSDUCTION MODEL

The electrostatic method utilizes a change in capacitance to either cause a voltage increase in a constant charge system, or a charge increase in a constant voltage system. This capacitance change can be used to pump energy into a storage capacitor. The

devices in this work maintain fixed capacitance geometries but modify the dielectric permittivity by using the mechanical energy of an evaporation-driven flow to move an alternating set of two fluids with two different dielectric constants between fixed plates. This is in contrast with the capacitive method used by vibration-based harvesting devices, where geometric parameters are modified to change the capacitance.

The constant charge implementation was selected for use in this work due to its simplicity over the constant voltage implementation, which would require an additional voltage source. The energy increase in the system as a result of each change in capacitance is given by equation (1).

$$\Delta E = E_{final} - E_{initial} \quad (1)$$

The constant charge implementation requires that the capacitance decrease from the initial value in order to harvest energy from the capacitance change. By noting that the variable capacitor can have a maximum value of C_{max} and minimum value of C_{min} , then the energy gained using the constant charge model can be represented by equation (2).

$$\Delta E = \frac{1}{2} (C_{max} - C_{min}) V_{max} V_{min} \quad (2)$$

3. DEVICE OPERATION

3.1 Overview of Operation

In the devices developed, a plant-like microfluidic network is used to maximize the flow rate due to evaporation. Evaporation can be caused by changes in multiple environmental conditions such as: (1) percent relative humidity, (2) temperature, (3) pressure, (4) volume of gas, (5) density of gas, and (6) flow rate of gas.

The mechanical energy of the evaporation driven flow moves a dielectric boundary to change the dielectric material between capacitive electrodes. The

Report Documentation Page

Form Approved
OMB No. 0704-0188

Public reporting burden for the collection of information is estimated to average 1 hour per response, including the time for reviewing instructions, searching existing data sources, gathering and maintaining the data needed, and completing and reviewing the collection of information. Send comments regarding this burden estimate or any other aspect of this collection of information, including suggestions for reducing this burden, to Washington Headquarters Services, Directorate for Information Operations and Reports, 1215 Jefferson Davis Highway, Suite 1204, Arlington VA 22202-4302. Respondents should be aware that notwithstanding any other provision of law, no person shall be subject to a penalty for failing to comply with a collection of information if it does not display a currently valid OMB control number.

1. REPORT DATE DEC 2008	2. REPORT TYPE N/A	3. DATES COVERED -			
4. TITLE AND SUBTITLE Evaporation-Driven Charge Redistribution And Current Generation For Energy Harvesting Applications		5a. CONTRACT NUMBER			
		5b. GRANT NUMBER			
		5c. PROGRAM ELEMENT NUMBER			
6. AUTHOR(S)		5d. PROJECT NUMBER			
		5e. TASK NUMBER			
		5f. WORK UNIT NUMBER			
7. PERFORMING ORGANIZATION NAME(S) AND ADDRESS(ES) Department of Electrical Engineering and Computer Science The University of Michigan Ann Arbor, MI, 48109		8. PERFORMING ORGANIZATION REPORT NUMBER			
		10. SPONSOR/MONITOR'S ACRONYM(S)			
9. SPONSORING/MONITORING AGENCY NAME(S) AND ADDRESS(ES)		11. SPONSOR/MONITOR'S REPORT NUMBER(S)			
		12. DISTRIBUTION/AVAILABILITY STATEMENT Approved for public release, distribution unlimited			
13. SUPPLEMENTARY NOTES See also ADM002187. Proceedings of the Army Science Conference (26th) Held in Orlando, Florida on 1-4 December 2008, The original document contains color images.					
14. ABSTRACT					
15. SUBJECT TERMS					
16. SECURITY CLASSIFICATION OF:			17. LIMITATION OF ABSTRACT SAR	18. NUMBER OF PAGES 8	19a. NAME OF RESPONSIBLE PERSON
a. REPORT unclassified	b. ABSTRACT unclassified	c. THIS PAGE unclassified			

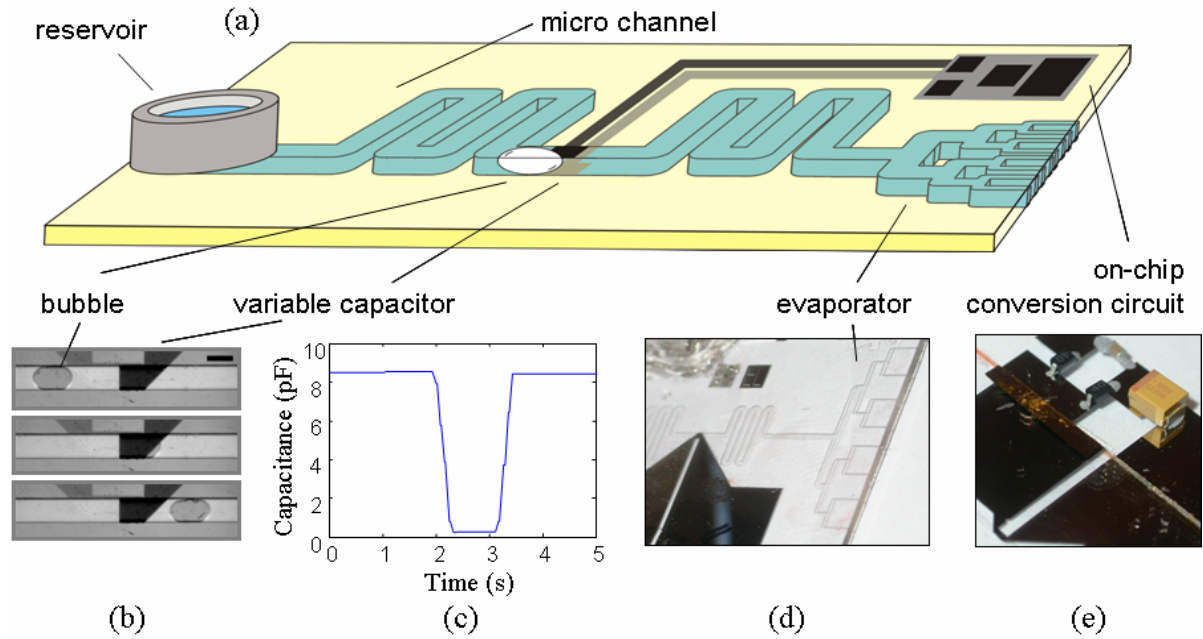


Figure 1. An overview schematic of the transpiration for electrical energy conversion device with close-up insets: (a) overview illustration showing water reservoir and meandering micro channel to allow for a long bubble train, (b) bubble transiting between capacitor plates (scale bar = 500 μm), (c) typical capacitance changes were from 8 – 10 pF for these devices for each bubble, (d) evaporator branching network, (e) surface mount conversion circuit.

change in the dielectric material results in a change in capacitance over the period of time that it takes for the boundary to traverse the capacitor electrode length, dC/dt . The change in capacitance is then converted to electrical power using a charge pump circuit.

An illustration of the energy conversion device is shown in Figure 1 along with various micrograph insets of each device component. The device consists of a parent channel which branches out mimicking plant microvasculature and following Murray's Law to optimize hydraulic conductance as shown in Figure 1(d) (McCulloh 2003). Fixed capacitor plates are fabricated into the top and bottom of the channel and fluid is moved between them. As a bubble traverses between the electrodes Figure 1(b), it causes the capacitance to decrease. The conversion circuit, shown in Figure 1e, uses diodes to conduct during capacitance decrease (at the leading bubble edge), and block current during capacitance increase (at the trailing bubble edge). The flow of the fluid is driven by evaporation, much like in plants, and as a result, is passive.

3.2. Device Materials

In addition to the microvasculature network shown in Figure 1, porous materials were also used as evaporators by placing them at the channel outlet in lieu of the etched glass bifurcating design, as shown in Figure 2. The material properties of each evaporator used in testing the device are given in Table 1. The main channel uses parylene as a dielectric insulator.

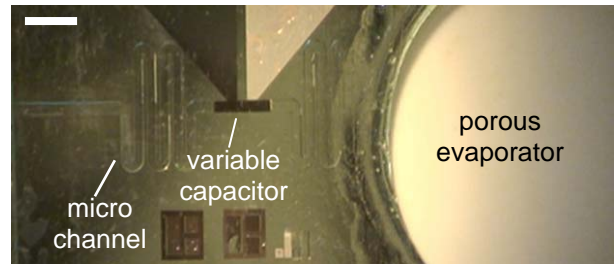


Figure 2. Micrograph of transpiration based energy conversion device with a porous ceramic evaporator at the channel outlet (scale bar = 3 mm).

Table 1. Properties of evaporator materials used

Evaporator Material	Pore Diameter (μm)	Void Volume %	Evaporative Surface Area (m^2)
$\frac{3}{4}$ Glass and $\frac{1}{4}$ Parylene	75	90	5.40×10^{-5}
Fired Alumina	6	50	3.17×10^{-4}
Fired Alumina	2.5	45	3.17×10^{-4}
Silica 99.99%	0.2	31	1.10×10^{-4}
Silica 99.99%	0.004	31	1.10×10^{-4}

3.3. Fabrication

The devices in this work were microfabricated on two glass wafers that were bonded to each other with a polymer (Figure 3). Microfabrication was used in order to achieve the same scale as plants such that capillary pressure dominates.

Microchannels were patterned and etched

isotropically in HF to achieve 45 - 75 μm channel depths in glass wafers. Capacitor plates were patterned on the bottom of the channels in wafer 1 shown in Figure 3 using an evaporated layer of titanium and platinum (300 \AA Ti/ 1000 \AA Pt). Similar Ti/Pt pads were patterned on wafer 2. That wafer was then diced and a layer of chrome and gold (200 \AA Cr/ 2000 \AA Au) was sputtered around the edge to create an electrical contact to the capacitor electrodes on the back side of the wafer. Then, wafer 2 was coated in 1.2 μm of Parylene C. Holes were manually drilled into wafer 2 using a drill press for fluidic interconnection to reservoir (not shown).

Wafers 1 and 2 were aligned then bonded using a stamping process and Sylgard 184 PDMS from Dow Corning. Surface mount components of the circuit were assembled soldered onto the Ti/Pt pads on wafer 1. Finally, the electrical contact of wafer 2 was wire-bonded to a pad on wafer 1. The devices that used a porous material as the evaporator followed the same process, with an additional step of gluing the porous material to the channel outlet using epoxy.

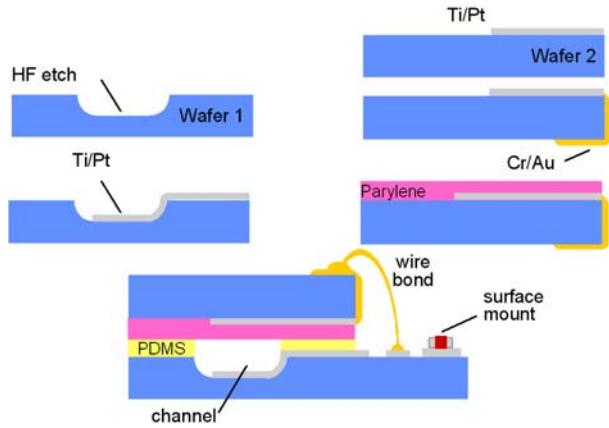


Figure 3. An illustration of the fabrication process of the transpiration based energy conversion devices.

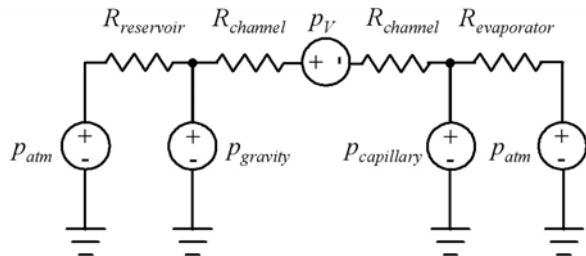


Figure 4. A lumped model representation of the fluidic network. The four sources of pressure shown are atmospheric (p_{atm}), gravitational ($p_{gravity}$), capillary ($p_{capillary}$), and electroosmotic pressure (p_V) due to the non-zero voltage on the capacitor plates. At the microscale, the evaporative pressure drop is dominated by the $p_{capillary}$ (i.e. $p_{capillary} \gg p_{atm}$ and $p_{gravity}$). It is known that p_V is also less than $p_{capillary}$ at channel radius values greater than 1 μm (Mutlu 2004).

4. EVAPORATION-DRIVEN FLOW

4.1 Change in Capacitance

The lumped element model analogy between fluidic and electrical linear element for the devices in this work is shown in Figure 4. The flow of liquid in the channel is dominated by the pressure drop to capillary openings at the end of the channel, $p_{capillary}$ (Eijkel 2005). Thus, the net liquid flow is from the reservoir to the evaporator. The existence of a non-zero voltage on the capacitor plates generates an electroosmotic pressure, p_V , however, for the devices in this work, this pressure was much less than the capillary pressure ($p_{capillary} > 200X p_V$).

4.2 Volumetric Flow Rate

The volumetric flow rate was measured in liters per minute and then normalized to the evaporative surface area (m^2) given in Table 1 in order to characterize the fluidic parameters of the biomimetic devices. The evaporative surface area was different for each evaporator pore diameter due to either fabrication limitations, as was the case for the 75 μm pore diameter evaporator, or due to limitations of the geometries available from the manufacturer, as was the case for the 4 nm, 200 nm, 2.5 μm , and 6 μm pore diameters. As shown in Figure 5, the highest average volumetric flow rate was obtained by the evaporator with 6 μm pore diameters and the lowest was obtained by the evaporator with 4 nm pore diameters.

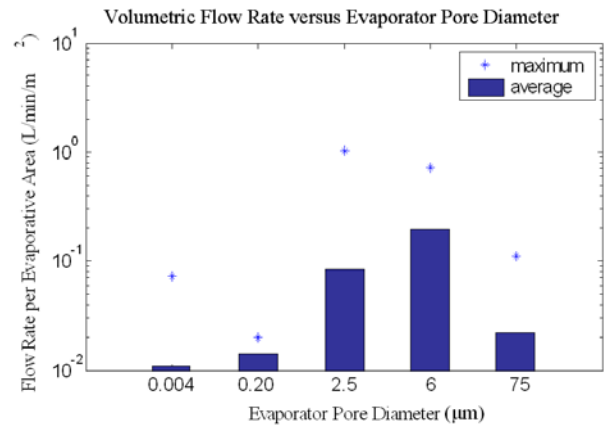


Figure 5. The average and maximum evaporation-driven volumetric flow rate normalized by the evaporative surface area for each evaporator pore diameter. Devices with pore diameters of 4 nm and 200 nm had an area of $1.1 \times 10^{-4} \text{ m}^2$, pore diameters of 2.5 μm and 6 μm had an area of $3.17 \times 10^{-4} \text{ m}^2$, pore diameters of 75 μm had an area of $5.4 \times 10^{-5} \text{ m}^2$. The devices with pore diameters of 75 μm were part of the branching network that obeyed Murray's Law and was etched in glass. Channel height = 45 μm and channel width = 500 μm .

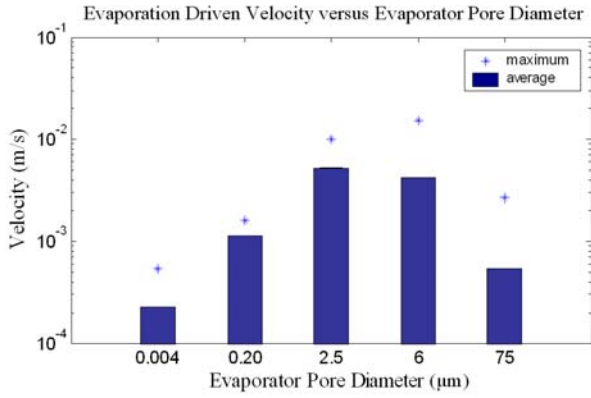


Figure 6. The average and maximum evaporation-driven velocity for each evaporator pore diameter tested: 4 nm, 200 nm, 2.5 μm, 6 μm, and 75 μm. Channel height, $h = 45 \mu\text{m}$ and channel width, $w = 500 \mu\text{m}$. Note that these measurements are not normalized by evaporative surface area to allow for comparison with the capacitor changes of individual devices.

For the devices in this work, the velocity with which the fluid in the channel traversed between the capacitor electrodes is a more important indicator of device performance due to the dependence of the output power on dC/dt . The velocity measurements are not normalized by evaporative surface area and are shown in Figure 6. The evaporators with 2.5 μm and 6 μm pore diameters exhibited the fastest velocities.

5. ELECTRICAL PROPERTIES

5.1 Change in Capacitance

At 1 MHz, the change in capacitance, ΔC_{var} , was consistently measured to range from 8 - 10 pF (Figure 1c) for the devices in this work. However, the measured change in capacitance has a dependence on measurement frequency, as shown in Figure 7, due to the fact that the relative dielectric permittivity of water varies nonlinearly with frequency.

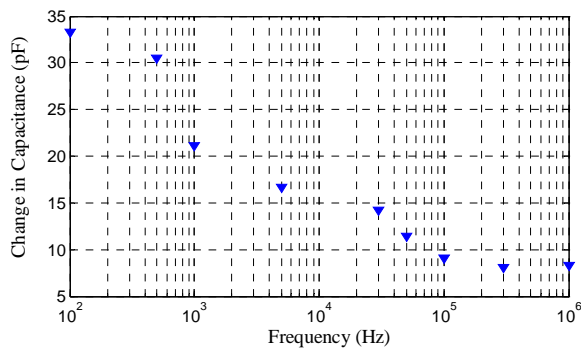


Figure 7. The measured change in capacitance, as the interface sweeps from water to air, versus measurement frequency.

At lower measurement frequencies ($f < 100 \text{ Hz}$), the relative dielectric permittivity of water has been measured to be approximately 6×10^5 . The maximum evaporation driven fluidic velocity for the devices in this work was measured to be $1.5 \times 10^{-2} \text{ m/s}$, thus, the frequency with which the bubbles can traverse through the capacitor electrodes ($l = 3 \text{ mm}$) is well into the high relative dielectric permittivity of water regime.

5.2 Current and Charge Modeling and Measurements

A charge redistribution circuit, shown in Figure 8, was used to measure the current from each water to air interface. In this circuit, a storage capacitor, C_{store} , is placed in parallel with the variable capacitor, C_{var} , and both capacitors are pre charged to a voltage, V_{in} . The voltage is applied when $C_{var} = C_{max}$, or when there is only water between the capacitor electrodes, then C_{var} is changed as bubbles traverse between the electrodes. With each bubble entrance, charge should transfer from C_{var} to C_{store} . With each bubble exit, charge should transfer from C_{store} to C_{var} . This is shown in Figure 9.

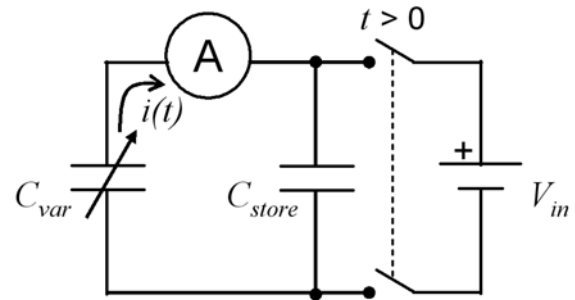


Figure 8. Charge redistribution circuit used to measure current and charge from each dielectric interface. The voltage source is disconnected at $t = 0 \text{ s}$. Current is measured as bubbles traverse between the electrodes.

As expected, the current and charge from each change in capacitance as a bubble traverses between the electrodes is not a function of input voltage, V_{in} , but only a function of the rate of change of capacitance, dC/dt , and the magnitude of the change in capacitance, ΔC_{var} . The results for the measured peak current, charge, and instantaneous power are shown in Figure 10. The measurements were conducted for three different flow rates. For the first flow rate (red line), the transpiration based device was configured using the 6 μm pore diameter evaporator disk at the channel outlet. Bubbles were then passively driven between the capacitor, and the current was measured between C_{var} and C_{store} . For the other two flow rates (blue and black lines), the device was connected to a syringe pump at the inlet and the outlet was simply open with no evaporator. This was used to quantify performance without environmental variability caused by discontinuities in evaporation.

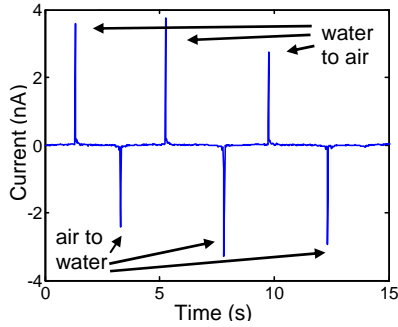


Figure 9. Measured current for multiple bubbles. A positive current is due to the leading bubble edge and the transfer of charge from the variable capacitor to the storage capacitor..

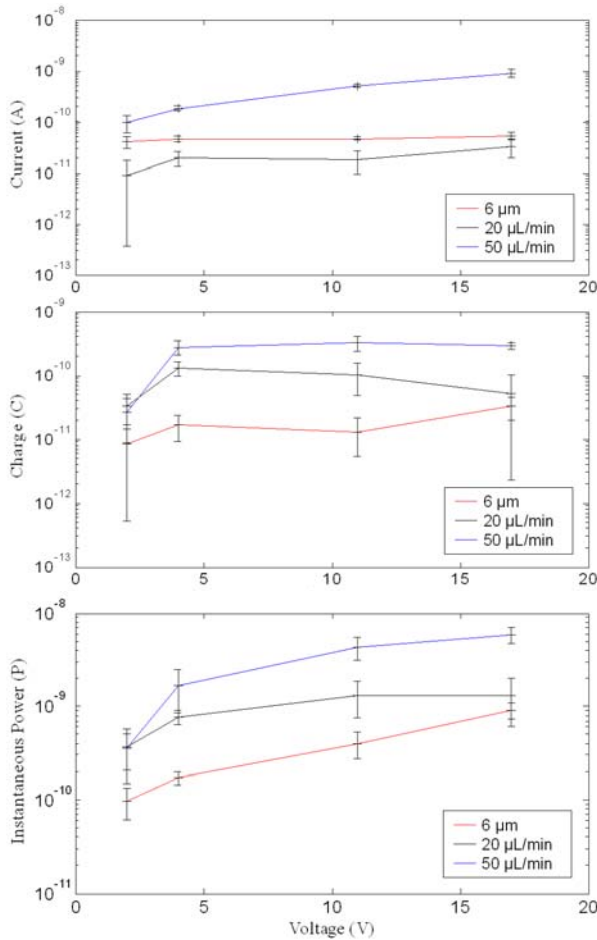


Figure 10. Measured results for (a) peak current, (b) charge, and (c) peak power, versus voltage. Three sources of fluid flow were used: (1) the evaporator with 6 μm pore diameters, (2) a syringe pump providing 20 $\mu\text{L}/\text{min}$ flow rate, and (3) a syringe pump providing a 50 $\mu\text{L}/\text{min}$ flow rate.

5.3 Scalability

The feasibility of scaling on this technology must be demonstrated in order to project the theoretical limits of this mechanism of energy conversion. Thus, two variable capacitor devices were connected in parallel

and then placed in the same charge redistribution circuit (Figure 8) used to measure current and charge. As can be seen in Figure 11, connecting multiple variable capacitors in parallel provides two benefits. The first being the increased refresh rate. At $t = 1$ s and $t = 1.5$ s, two positive spikes are shown indicating that a bubble entered C_{var1} at $t = 1$ s, and another entered C_{var2} at $t = 1.5$ s. Thus, instead of requiring very high flow rates, each device could spike at different times and simulate a faster flow rate. The second benefit is the additive effect. If the bubbles in both C_{var1} and C_{var2} enter between the capacitor electrodes at the same time, then the current measured would be double that of one bubble in one device. This can be seen at $t = 4$ s, where the peak current is approximately 2×10^{-9} A.

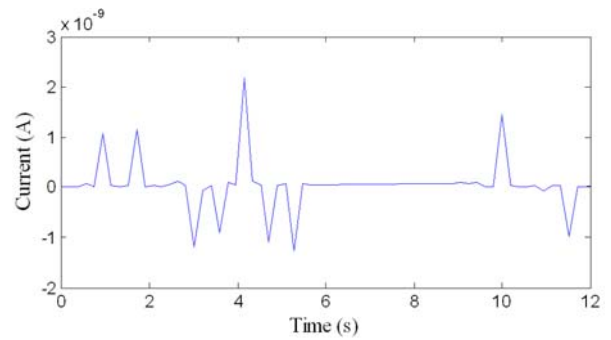


Figure 11. Current versus time showing scalability of energy conversion by connecting two devices in parallel in the charge redistribution circuit.

5.4 Voltage Pump Circuit Theory

The true application of the presented transpiration based energy conversion mechanism is as an energy scavenging supply. Thus, a full conversion circuit that is capable of transducing the mechanical energy in the evaporation-driven fluid into electrical power is necessary. This circuit, as with any other, will include some inherent losses. However, if the change in capacitance, or ΔC_{var} , can be made large enough, or if the change can occur more quickly to maximize dC/dt , then the energy harvested from this mechanism can overcome the leakage in the circuit and potentially allow for the harvesting and storage of additional energy. Similar voltage output conversion circuits used in the transpiration based work here have been used in vibration energy harvesting devices (Tashiro 2002). Other well-known energy conversion circuits developed for electrostatic energy harvesting devices have been optimized for periodic signals from high frequency vibrations (Meninger 2001) and thus, include clocks for timing references. As discussed, many environmental conditions affect the rate of evaporation. As a result, periodic changes in capacitance are not possible with a transpiration based energy harvesting mechanism.

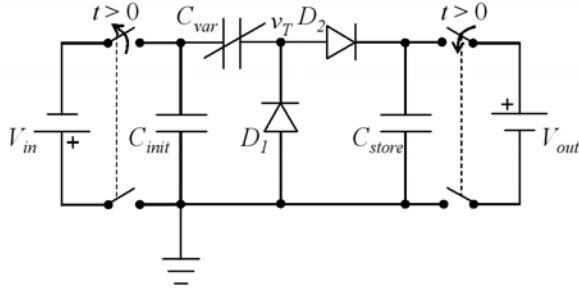


Figure 12. A schematic of the output voltage conversion circuit implemented in the transpiration based energy harvesting devices in this work. The initial capacitor, C_{init} , and the variable capacitor, $C_{var} = C_{max}$, are pre-charged to $-V_{in}$. The power supply is then disconnected at $t = 0$ s.

In the initial condition, the value of the variable capacitor is set to $C_{var} = C_{max}$ and both C_{var} and the initial capacitor, C_{init} , are charged to a negative initial voltage. The total energy in the system is given by (3) and (4) as the sum of the energy in each capacitor. The energy stored on a capacitor at any time is a function of the voltage across that capacitor at that time, and V_{out} on C_{store} starts at 0 V.

$$E_{Total} = E_{init} + E_{var} + E_{store} \quad (3)$$

$$E_{Total} = \frac{1}{2} C_{init} V_{in}^2 + \frac{1}{2} C_{var} V_{in}^2 + \frac{1}{2} C_{store} V_{out}^2 \quad (4)$$

When a bubble enters between the electrode plates of C_{var} and changes its value from C_{max} to C_{min} , then ΔC_{var} results in an increase of V_{out} on C_{store} . The positive current due to a decrease in the capacitance of C_{var} results in a positive charge that is conducted by the diode, D_2 , to C_{store} .

When a bubble exits from the electrode plates of C_{var} and changes its value from C_{min} to C_{max} , there is no voltage accumulation on V_{out} . However, at this point, a full energy conversion cycle has occurred and the system has a net positive energy gain, ΔE_{cycle} , as given by equation (5).

$$\Delta E_{cycle} = \frac{1}{2} C_{store} V_{out}^2 \quad (5)$$

5.5 Voltage Pump Circuit Testing

For testing purposes, PTFE tubing was loaded with alternating sections of water and air bubbles to provide a large number of dielectric interfaces. The tubing was connected to a syringe that was loaded into a syringe pump to deliver a volumetric flow rate of 100 $\mu\text{L}/\text{min}$.

The circuit in Figure 12 was pre-charged to a voltage of -5 V when only water was between the variable capacitor electrodes (i.e. $C_{var} = C_{max}$) and then the voltage source was disconnected. The output voltage on C_{store} was then measured and a microscope and camera were used to record video of the bubbles traversing between the capacitor plates and synchronize them with the measured output voltage.

The measured output voltage, V_{out} on C_{store} , is shown in Figure 13. The output voltage is first measured for a few seconds with only water in between the variable capacitor plates ($C_{var} = C_{max}$ and $dC_{var}/dt = 0$). Note that the output voltage starts at a nominal voltage of approximately 0.95 V, ideally, this should be 0 V. The output voltage then decays slowly as a result of the impedance of the measurement instrument. When the syringe pump is switched on at around $t = 30$ s, bubbles begin to traverse between the variable capacitor electrodes causing C_{var} to change from C_{max} to C_{min} and back to C_{max} . Each leading bubble edge results in an increase in output voltage of approximately 2 - 5 μV . This data demonstrates that voltage pumping is possible in a real circuit with diode leakage, capacitor leakage due to parasitic resistances, as well as other interconnect and resistive parasitics.

In Figure 14, the output voltage starts at $V_{out} = 0$ V and $t = 0$ s. This is to show what the output would look like if bubbles started going between the variable capacitor electrodes as soon as measurement began. These measured data still take into account the leakage in the circuit and shows that voltage accumulation can occur with the presented mechanism for mechanical to electrical energy conversion. The output voltage is also directly compared with the simulation results. Good agreement is seen between simulation (ideal and actual diode) and measured results, as is the energy on the storage capacitor, E_{store} (Figure 15).

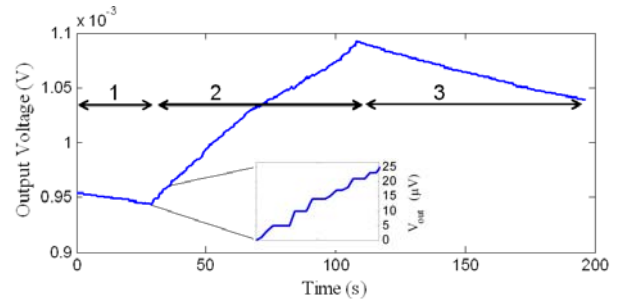


Figure 13. The measured output voltage. In region 1, $C_{var} = C_{max}$. In region 2, many bubbles are traversing between the electrodes. C_{var} is changing from C_{max} to C_{min} at a rate set by a syringe pump at 100 $\mu\text{L}/\text{min}$. In region 3, only water is in the electrodes and $C_{var} = C_{max}$ and shows natural decay at the output in this region. The close up inset shows the steps due to individual bubbles.

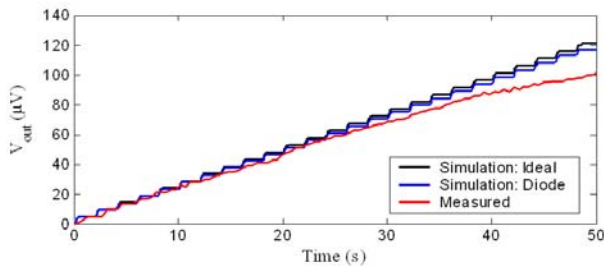


Figure 14. The measured voltage output, V_{out} , plotted such that $V_{out} = 0$ V at $t = 0$ s. This measurement is compared to the simulation results for both ideal and the actual diode. These data show that voltage accumulation can occur even with inherent leakage in the system.

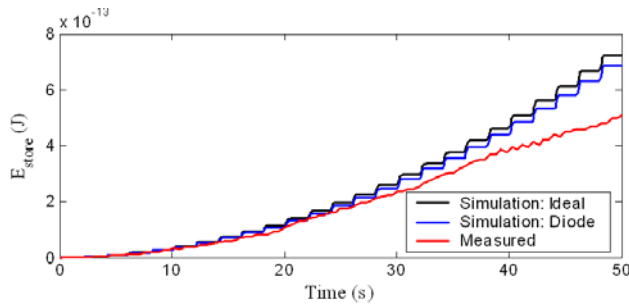


Figure 15. The measured energy, E_{store} , on the storage capacitor, C_{store} , compared to the simulation results both ideal and the actual diode.

Table 2. The output voltage per second as a function volumetric flow rate.

Volumetric Flow Rate ($\mu\text{L}/\text{min}$)	$\Delta V_{out}/\text{second}$ (V/s)
100	$2.0 \times 10^{-6} - 5.0 \times 10^{-6}$
20	0
5	-1.00×10^{-6} , baseline leakage
0	-1.00×10^{-6} , baseline leakage

A summary of the output voltage per second as a function of volumetric flow rate is shown in Table 2. This table highlights that in order to overcome the baseline leakage, a minimum flow rate of 20 $\mu\text{L}/\text{min}$ is necessary.

5.6 Theoretical Limit

5.6.1 Limit Due to Geometric Parameters

The theoretical limit of this technology depends on the size of the leading bubble edge interface. As shown in Figure 16, the minimum variable capacitor length to allow for a change in capacitance from C_{max} to C_{min} by a leading bubble edge is 150 μm . Therefore, the minimum area, A_{min} , required for each variable capacitor is approximately $7.5 \times 10^{-8} \text{ m}^2$.

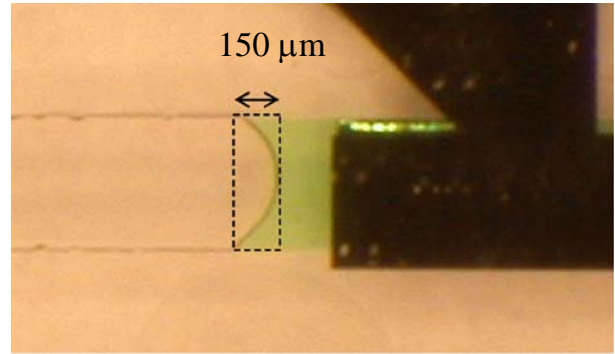


Figure 16. Micrograph showing the leading edge of a bubble. The meniscus radius gives an idea of the minimum variable capacitor length that can be used in a transpiration based energy harvesting system.

5.6.2 Limit Due to Leakage of Initial Capacitor

Two modes of operation for an energy harvesting device can be defined when it is used to power an electronic device (Mateu 2005). The first is when the power consumption of electronic device is less than the power provided by the energy harvester. The second is when power consumption of the electronic device is larger than the power provided by the energy harvester. The second case is the more likely case if the transpiration-based energy harvesting device were implemented. Thus, the operation of the electronic device that is suitable is a discontinuous one. For example, a sensor that takes a measurement once a day or once an hour. Further, for discontinuous modes of operation, it is more useful to describe the energy generated rather than the power generated because the energy sets the time limit between device operation.

The limiting component for energy efficiency is the initial capacitor. This capacitor has a finite resistive path to ground. The magnitude of that resistance will determine how quickly the initial capacitor will lose charge and require a refresh from another power supply, battery, or capacitor. For the devices in this work, the initial capacitor had a manufacturer specified parallel resistance of 10 G Ω . However, for illustrative purposes, an exaggerated leakage model with a small parallel resistance on C_{init} is used to discuss the energy efficiency requirements of the transpiration-based energy conversion device should it be used as a stand alone energy harvester. With a small resistance value of 10 M Ω , we expect that the charge on the initial capacitor will drain quickly. An example of the loss of V_{init} on C_{init} is given in Figure 17(top), which will result in an output voltage, V_{out} , on C_{store} as shown in Figure 17(bottom). Even if the variable capacitor is still changing (i.e. bubbles are still traversing between the variable capacitor electrodes), no output voltage can be accumulated if $V_{init} = 0$ V. Obviously, a capacitor with a 10 G Ω parasitic resistance will discharge 1000X slower, or in approximately $30 \text{ s} \times 1000 = 8.3$ hours.

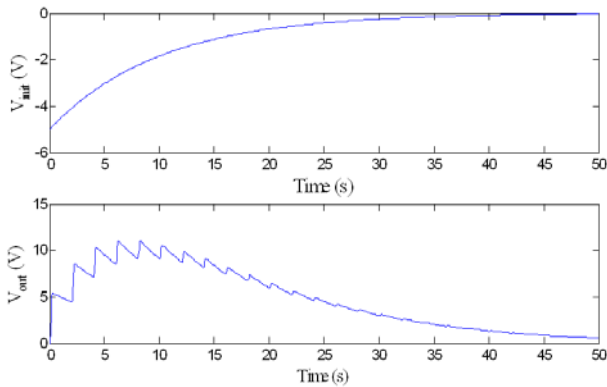


Figure 17. (top) The initial voltage, V_{init} , and (bottom) output voltage, V_{out} , on C_{init} and C_{store} , respectively, due to a high leakage from a small parallel resistance on C_{init} . This example uses an exaggerated leakage resistance to illustrate the refresh requirement concept. In this case, there is no refresh of the initial voltage and it slowly drains to 0 V.

Some overhead electronics will be included in order to regulate a refresh circuit in an actual implementation of this technology as a stand alone energy harvesting device. Many researchers have studied the control electronics for this purpose and it is a topic of ongoing investigation (Meninger 2001, Host-Madsen 2005).

An example of simulation results of the recharge on V_{init} is given in Figure 18(top) yielding an output voltage, V_{out} , shown in Figure 18(bottom). Based on these simulations, the percent efficiency of this technology as a stand alone energy harvesting device can be calculated as a function of the final energy of the system and the sum of the initial energy in the system, plus the energy requirement of the overhead electronics to refresh the initial voltage on C_{init} . Based on simulation results for efficiency, a bound can be set for the maximum energy consumption of the overhead electronics in order to achieve a percent efficiency great than 0%. At small C_{store} values such as 1 nF, the energy harvesting mechanism would achieve negative efficiency, meaning that more energy is input into the system than is being harvested out. The energy consumption of the overhead electronics should be less than 1 μ J per refresh cycle in order to achieve a percent efficiency greater than 0% for a $C_{store} = 20$ nF. For comparison, a single 0.25 μ m MOSFET running at 5 V would have an energy consumption of approximately $0.5 \times C_{gate} V^2 = 1/2 \times 5 \text{ fF} \times 5^2 = 62.5$ fJ.

The efficiency of the transpiration based mechanism as a stand alone energy harvesting device will be determined by the requirements of the overhead electronics and the device that will be powered by the energy harvester. Further exploration of this topic is necessary in any future research of transpiration based energy harvesting mechanisms.

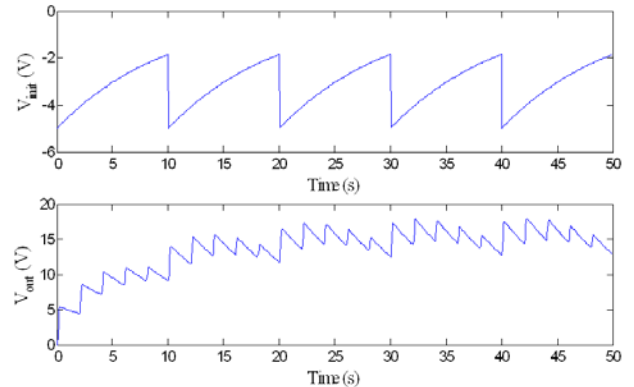


Figure 18. (top) The initial voltage, V_{init} , and (bottom) output voltage, V_{out} , on C_{init} and C_{store} , respectively, using a refresh circuit to recharge the voltage, V_{init} , on C_{init} . This example uses an exaggerated leakage resistance to illustrate the refresh requirement concept and the initial voltage is refreshed every 10 seconds.

6. DISCUSSION

A novel mechanism for electrical energy conversion from evaporation-driven motion was presented. The device was inspired by the microvasculature in plants. The microfluidic nature of the design was characterized and enhanced using porous material as evaporators. Devices were coupled to show that the outputs can be added and that multiple devices can either increase the refresh rate or increase the magnitude of the output current. Output voltages of 2 – 5 μ V were measured for each leading bubble edge, providing a proof of concept demonstration for the use of a transpiration-based energy conversion mechanism. Current work focuses on replacing the gas bubbles with solid, entrapped dielectrics to generate a system which can scavenge continuously without any user intervention.

REFERENCES

- Borno, R. T., et. al., "Energy scavenging from transpiration," *11th Int'l Conf. on MicroTAS*, Paris, pp. 566-568, Oct. 2007.
- Eijkel, J. C. T., et. al., "Water in micro- and nanofluidics systems described using the water potential," *Lab on a Chip*, vol. 5, pp. 1202-1209, 2005.
- Host-Madsen, A., and Zhang, J., "Capacity bounds and power allocation for wireless relay channels," *IEEE Transactions on Information Theory*, vol. 51, pp. 2020-2040, 2005.
- Mateu, L., and Moll, F., "Review of energy harvesting techniques and applications for microelectronics," *Proc. SPIE Microtechnologies for the New Millennium*, Sevilla, Spain, pp. 359-373, 2005.
- McCulloh, K. A., et. al., "Water transport in plants obeys Murray's Law," *Nature*, vol. 27, pp. 939-942, 2003.
- Meninger, S., et. al., "Vibration to electric energy conversion," *IEEE Transactions VLSI Systems*, vol. 9, pp. 64-76, 2001.
- Mutlu, S., "Microfluidic Biochemical Analysis System With Electro-Osmotic Pump and Thermally Responsive Polymer Valve," Ph.D. Dissertation, University of Michigan-Ann Arbor, 2004.
- Tashiro, R., et. al., "Development of an electrostatic generator for a cardiac pacemaker that harnesses the ventricular wall motion," *Journal of Artificial Organs*, vol. 5, pp. 239, 2002.